

PROMPT PHOTON PLUS CHARM PRODUCTION AT NEXT-TO-LEADING ORDER IN QCD

B. BAILEY

Physics Department, Eckerd College, St. Petersburg, FL 33711, U.S.A.

E. L. BERGER and L. E. GORDON

*High Energy Physics Division, Argonne National Laboratory,
Argonne, IL 60439, U.S.A.*

The two particle inclusive cross section for the reaction $p + \bar{p} \rightarrow \gamma + c + X$ is studied in perturbative quantum chromodynamics at order $O(\alpha_s^2)$. Differential distributions are provided for various observables, and a comparison is made with data from the CDF collaboration.

1 Introduction

Theoretical study of the reaction $p + \bar{p} \rightarrow \gamma + c + X$ is interesting for several reasons. The two particle inclusive cross section probes QCD dynamics in more detail than a single particle inclusive cross section. Specification of the cross section in next-to-leading order in QCD is correspondingly more challenging, and data will permit a study of various correlations including those in the rapidities and transverse momenta of the final photon and charm quark. Second, the data may permit a direct measurement of the charm quark density of the proton if it can be shown, as we do^{1,2}, that the hard scattering cross section is dominated by the contribution from the cg scattering subprocess, where the incident c quark is a constituent of one of the initial hadrons. Third, it is valuable to be able to compare data obtained by the CDF Collaboration³ on prompt photon production in association with charm decay products, such as e^\pm , μ^\pm and D^\pm , with next-to-leading order predictions.^a

We have published two next-to-leading order calculations in perturbative QCD of the reaction $p + \bar{p} \rightarrow \gamma + c + X$ at collider energies^{1,2}. In most of the data of interest, the charm quark carries a relatively large value of transverse momentum, $p_T^c \geq 10$ GeV. Since this value is large when compared

^aInvited paper presented by E. L. Berger at the 28th International Conference on High Energy Physics, Warsaw, Poland, July 25 - 31, 1996. Argonne report ANL-HEP-CP-96-84. This work was supported by the US Department of Energy, Division of High Energy Physics, Contract no. W-31-109-ENG-38.

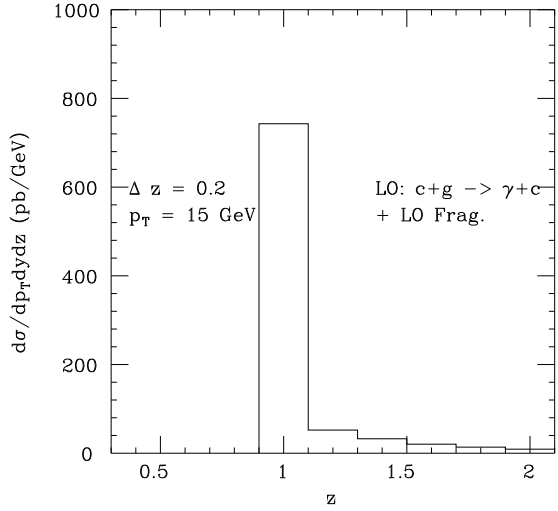


Figure 1: Cross section as a function of z at $y^\gamma = 0$ in leading order.

to the mass of the charm quark, we neglect the mass of the quark, and we include hard-scattering subprocesses in our calculation in which the charm quark is a constituent of the initial hadrons. For values of p_T^c less than 10 GeV or so, it would be necessary to retain a finite mass for the quark and to examine a different set of subprocesses in which the massive quark is not a constituent in the initial state but is, instead, produced in the hard scattering⁴. A calculation with $m_c \neq 0$ also requires resummation of logarithmic terms of the form $\alpha_s^n \ln^n(p_T^c/m_c)$ for large values of p_T .

In leading-order, the contributions to associ-

ated production include the direct term $c + g \rightarrow \gamma + c$ along with several photon fragmentation processes typified by the hard scattering subprocess $c + q \rightarrow c + q$ followed by long-distance fragmentation of the final q into a photon: $q \rightarrow \gamma + X$. In next-to-leading order, there are gluon-exchange loop corrections to the lowest-order direct process, real gluon emission radiative corrections to the lowest-order direct process, and several new three-body final-state contributions: $g + g \rightarrow c + \bar{c} + \gamma$, $q + \bar{q} \rightarrow c + \bar{c} + \gamma$, $c + q \rightarrow c + q + \gamma$, $c + \bar{q} \rightarrow c + \bar{q} + \gamma$, $c + \bar{c} \rightarrow c + \bar{c} + \gamma$, and $c + c \rightarrow c + c + \gamma$. We include all of these. In principle, we should also include fragmentation to next-to-leading order. However, in view of the small size of the fragmentation contribution and the theoretical problems identified⁵ with isolated prompt photon production in next-to-leading order, we treat the fragmentation terms at lowest order.

The distinction between our two calculations^{1,2} resides in the different techniques used in performing the phase-space integrals. In the first paper, we insist on going as far as we can using purely analytical techniques. In the second, we use a combination of analytical and Monte Carlo techniques⁶. The second approach allows implementation of isolation cuts and other experimentally relevant selections. In both cases, we evaluate the gluon exchange and the real gluon emission diagrams analytically, expose the infrared and collinear singularities, cancel the infra-red singularities, and factor the collinear singularities into incident parton densities or final-state fragmentation functions. We use dimensional regularization to deal with the singularities. Although somewhat restrictive, the purely analytic calculation¹ provides the size of the two-particle inclusive cross section, the relative importance of various contributing subprocesses, and an important check on the more versatile combination² of analytic and Monte Carlo methods.

Some of our analysis is done in terms of the variable $z = -\vec{p}_T^c \cdot \vec{p}_T^\gamma / (p_T^\gamma)^2$, and some of the results are presented as histograms in z for finite intervals in z . If z is positive, the photon and charm quark are in opposite hemispheres. If $z = 1$, the photon and charm quark have equal and opposite values of transverse momentum. This situation occurs for the leading-order direct process, for gluon exchange loop corrections to the leading-order direct process, whenever an emitted

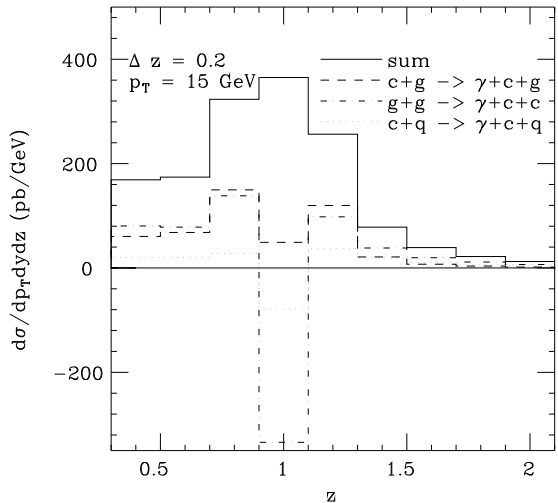


Figure 2: Cross section as a function of z in next-to-leading order. The dominant contributions are shown.

gluon becomes soft, and when a third parton in a three-parton final-state process becomes collinear to an incident parton. The point $z = 1$ is associated with various soft and collinear poles, exposed when the cross section is expanded as a function of z . The singularities are expressed in terms of delta functions, $\delta(1 - z)$, and “plus”-distributions, $1/(1 - z)_+$. The singularities are integrable, and results are expressed as integrals over finite intervals in z .

2 Numerical Results

Our results are presented at a center-of-mass energy $\sqrt{s} = 1.8$ TeV. The renormalization and factorization scales are taken as $\mu = p_T^\gamma$. We sum over charm and anticharm production throughout. In Fig. 1 the net lowest-order contribution is shown as a function of z at $p_T^\gamma = 15$ GeV. The lowest order cross section is made up of the lowest order direct term $cg \rightarrow \gamma c$, proportional to $\delta(1 - z)$, and fragmentation contributions. In Fig. 1, the direct term provides the peak at $z = 1$, and the various photon fragmentation terms contribute in the region $z \geq 1$. Note the absence of any contribution in the region $z < 1$, an unrealistic prediction that illustrates the inadequacy of the lowest order approach. The cross section in z resulting from our the next-to-leading order massless-charm calculation is displayed in Fig. 2. The next-to-leading or-

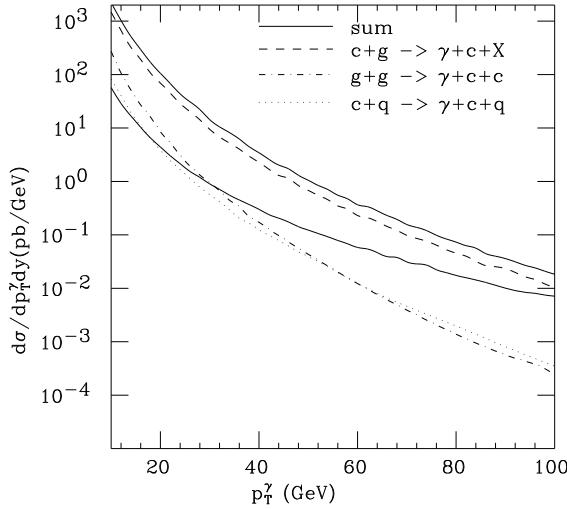


Figure 3: The transverse momentum dependence of $d\sigma/dp_T^\gamma dy^\gamma dz$, for z integrated over the interval $0.2 < z < 2.0$. The upper solid line shows the sum of all subprocesses through next-to-leading order. The dashed line shows the sum of the $O(\alpha_s)$ and $O(\alpha_s^2)$ contributions from the cg initial state. The $O(\alpha_s^2)$ contributions from the gg and cq initial states are shown as dash-dot and dotted curves. The lower solid line shows the $O(\alpha_s^2)$ contribution from the $\bar{q}q$, $\bar{c}c$, and cc initial states.

der collinear initial-state contributions reduce the peak at $z = 1$, and the next-to-leading order three-parton final-state contributions broaden the distribution. The cross section is finite at all values of z , similar to the situation observed in experiments. In Fig. 2 we also present the individual contributions from the most important subprocesses. The cg initiated process dominates the cross section, but there are important contributions from the gg and cq initiated subprocesses in the region of small p_T^γ . The predicted distribution in p_T^γ is shown in Fig. 3. As might be expected, the contribution from the $\bar{q}q$ initial state begins to become important at large p_T^γ .

Distributions in p_T^c and in the rapidities of the γ and c quark may be found in our publications^{1,2}. In the second paper, we also discuss the influence of photon isolation, and we compare the magnitude and shape of the next-to-leading order and leading order cross sections for various observables. As an example, we present Fig. 4, a distribution in p_T^c for different selections on z and the isolation cone variable R .

Positive correlations in rapidity at collider

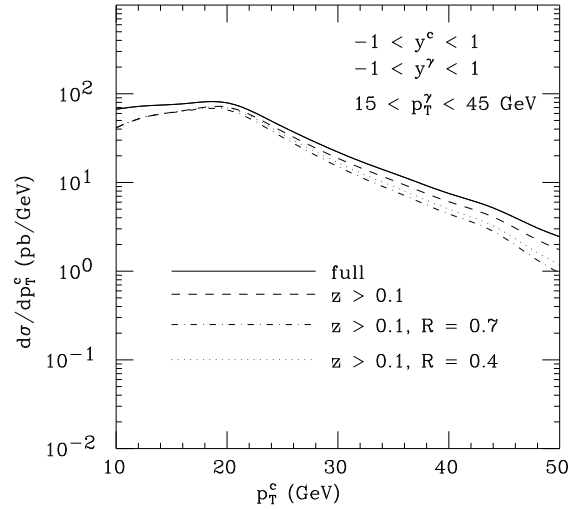


Figure 4: Cross section $d\sigma/dp_T^c$ as a function of p_T^c , with $15 < p_T^\gamma < 45$ GeV, and the rapidities of the photon and charm quark restricted to $-1.0 < y < 1.0$. The solid curve shows the cross section with no further restrictions and the dashed curve the result after the additional selection $z > 0.1$. The dotted and dash-dot curves display the results after photon isolation restrictions are applied, in addition to the cut on z .

energies are a dynamical property of the hard-scattering matrix element⁷. Indeed, it may be shown⁷ that the parton-level matrix element is proportional to $\cosh^{-1}(\Delta y)$, where Δy is the difference in the rapidities of two final-state particles in a two-particle inclusive reaction. In Fig. 5, we present the distribution in the difference of the rapidities of the photon and charm quark. In this example, the γ is selected to have rapidity in the forward region $1 < y^\gamma < 2$. Under these circumstances, as may be observed in Fig. 5, the charm quark is predicted to have positive rapidity also, with $\Delta y = y^\gamma - y^c$ peaking a value only slightly larger than 0.

In Fig. 6 we compare our results to CDF data⁸ for photon plus μ^\pm production, where the μ^\pm is identified as the decay product of a charm quark. The three upper points are obtained⁸ from the Monte Carlo event-generator Pythia whereas the lower point is our theoretical expectation. The Pythia cross section lies substantially below the data while our cross section exceeds the data somewhat.

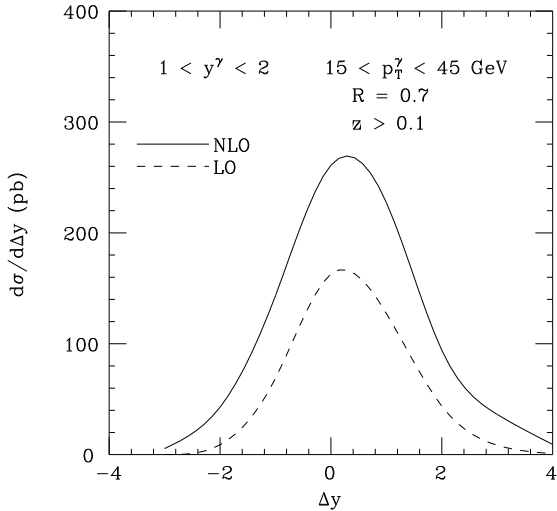


Figure 5: Cross section $d\sigma/d\Delta y$ as a function of the difference $\Delta y = y^\gamma - y^c$ of the rapidities of the photon and charm quark, for $p + \bar{p} \rightarrow \gamma + c + X$ at $\sqrt{s} = 1.8$ TeV. The ratio z is restricted to $z > 0.1$, and photon isolation is imposed, with $R = 0.7$. The transverse momentum and rapidity of the photon are selected to be in the intervals $15 < p_T^\gamma < 45$ GeV and $1.0 < y^\gamma < 2.0$. The dashed curve shows the behavior at leading order.

3 Conclusions

We presented the results of next-to-leading order QCD calculations of the inclusive production of a prompt photon in association with a charm quark. The two-particle inclusive cross section allows more refined tests of the underlying QCD dynamics, revealed, e.g., through rapidity correlations. Our cross section shows the expected reduced dependence on the choice of the factorization/renormalization/fragmentation scale in QCD. The sensitivity of the cross section to the charm quark content of the proton is preserved in next-to-leading order. A comparison with the CDF data shows reasonable agreement. Further work is underway to include effects associated with the finite mass of the charm quark and with charm fragmentation: $c \rightarrow DX$ or $c \rightarrow \mu X$. In other work, we are investigating associated production of photons and charm quarks at HERA energies and the associated production of photons and bottom quarks at collider energies.

References

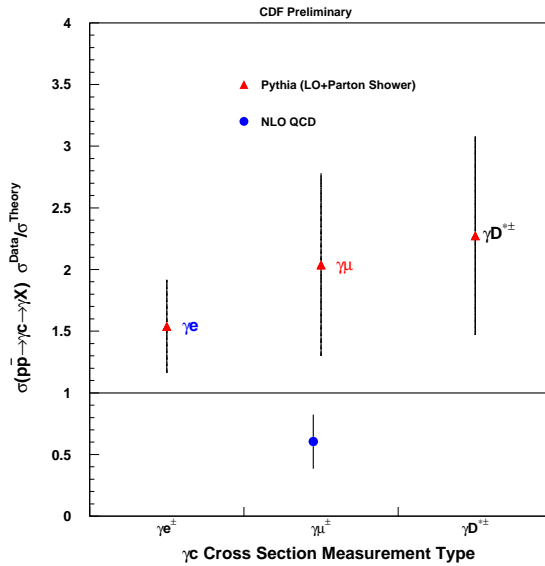


Figure 6: Ratio of the measured γcX cross section to that predicted, for various charm decay channels.

1. E. L. Berger and L. E. Gordon, *Phys. Rev. D* **54**, 2279 (1996) and references therein.
2. B. Bailey, E. L. Berger and L. E. Gordon, *Phys. Rev. D* **54**, 1896 (1996) and references therein.
3. CDF Collaboration, F. Abe *et al*, Fermilab Report FERMILAB Pub-96/152E, Submitted to *Phys. Rev. Lett.*
4. P. Nason, S. Dawson, and R.K. Ellis, *Nucl. Phys. B* **303**, 607 (1988); **327**, 49 (1989); **335**, 260 (1990) (E). W. Beenakker, H. Kuijif, W.L. van Neerven, and J. Smith, *Phys. Rev. D* **40**, 54 (1989); W. Beenakker, W.L. van Neerven, R. Meng, G.A. Schuler, and J. Smith, *Nucl. Phys. B* **351**, 507 (1991).
5. E. L. Berger, X. Guo, and J. W. Qiu, *Phys. Rev. Lett.* **76**, 2234 (1996); *Phys. Rev. D* **54**, (1996) (1 November, 1996).
6. B. Bailey, J. Ohnemus, and J. F. Owens *Phys. Rev. D* **46**, 2018 (1992).
7. E. L. Berger, *Phys. Rev. D* **37**, 1810 (1988).
8. S. Kuhlmann, CDF Collaboration, private communication.